Heliyon 9 (2023) e14226

Contents lists available at ScienceDirect

Heliyon

journal homepage: www.cell.com/heliyon

Research article

Performance analysis of the evacuated tube counter-flow absorber and direct-flow absorber to optimize the heat extraction rate for high flow rate applications

Shaibu Tambula *, Downmore Musademba, Chido H. Chihobo

Department of Fuels and Energy Engineering, Chinhoyi University of Technology, P. Bag 7724, Chinhoyi, Zimbabwe

ARTICLE INFO

Keywords:
Evacuated tube collector
Direct-flow absorber
Counter-flow absorbers
Heat extraction rate
Industrial solar heating

ABSTRACT

The evacuated tube collector (ETC) has gained extensive use in low-temperature applications due to its cheapness and high efficiency. The ETC can be used with a concentrator for medium temperature applications, in the range of 140–200 °*C*. However, the heat extraction rate of the absorber tube is a limitation factor, particularly at higher heat flux and high flow rates. The energy gained is not directly proportional to the concentration factor used. This work thus proposes a counter-flow copper absorber for increasing the heat extraction rate and compares its performance to the conventional direct-flow absorber. The designs are both optimized by varying the absorber diameters, and a material property analysis is done. COMSOL Multiphysics is used for the simulations. The performance of the 2 systems is evaluated using a conjugate heat transfer model at flow rate ranges of 0.02–0.2 kg/s and uniform theoretical heat flux of 1000, 2000, and 3000 W/m^2. Analysis of the results indicates that the counter-flow with 0.01 and 0.02 m inner and outer diameter respectively has 4 times more energy gain than the direct-flow with a 0.01 m diameter. Increasing the heat flux by 2 at 0.02 and 0.2 kg/s flow rate increases the temperature by 1.5 and 1.1 for the counter-flow absorber and 1.2 and 1.04 for the direct-flow absorber. Tripling the heat flux at the same flow rate range increases the temperature by 2 and 1.4 for the counter-flow absorber and 1.5 and 1.07 for the direct-flow absorber. The counter-flow absorber is thus the best choice at higher heat flux and high flow rates which are typically required for industrial heating.

1. Introduction

Solar energy presents opportunities in supplying sustainable energy for industrial heating, safeguarding natural resources, and offsetting carbon emissions. The ETC has gained extensive use in low-temperature applications, typically below 100 °*C*, due to its cheapness and high efficiency. According to Sabiha et al. [1], ETC is capable of generating up to 200 °*C* and can therefore be used in industrial heating. Several industries require medium temperatures in the range of 140–200 °*C*, these include the tea industry, sugar refineries, milk processing, and breweries. However, the temperature gained by the ETC reduces with a rise in flow rate, of which industrial heating is characterized by high flow rates. In solar collectors low flow rates lead to higher collector average temperatures, conversely, higher flow rates lead to fluctuating collector outlet temperatures. The high fluctuations result in the inability to

* Corresponding author. ;
E-mail addresses: stambula@cut.ac.zw (S. Tambula), dmusademba@cut.ac.zw (D. Musademba), chihobo@gmail.com (C.H. Chihobo).

https://doi.org/10.1016/j.heliyon.2023.e14226
Received 15 November 2022; Received in revised form 23 February 2023; Accepted 27 February 2023
Available online 1 March 2023
2405-8440/

continuously transport heat and a consequent increase in heat loss [2]. The ETC used in combination with a concentrator increases the outlet temperature, giving solar heating a high chance of penetrating industrial heating. The major challenge with ETC application is heat extraction from the single-ended, long, narrow borosilicate glass tube [3]. Furthermore, the cost of a solar thermal system is usually unattractive to industries due to high initial costs and high payback periods. A solar thermal system, therefore, needs to follow a simple design that is easy to manufacture and with low-cost materials but maintains high thermal efficiency. Enhancing the heat gain capacity is necessary to increase the efficiency of the ETC [4]. This can be done by improving the heat transfer capacity of the absorber.

The most frequently used absorbers for the ETC are the heat pipe, all-glass counter-flow absorber, and U-tube (direct-flow) absorber. The performance of the heat pipe absorber is affected by the viscous limit, entrainment limit, boiling limit, sonic limit, and capillary limit. Praful et al. [5] state that heat pipe must be meticulously designed for precise temperature ranges due to the relationship between the maximum heat transport capacity and operating temperature. In addition, the heat pipe is more expensive than a direct-flow absorber [6]. The direct-flow absorber is cheaper and can use water directly which can reduce its cost, however, the heat extraction rate is lower compared to the heat pipe absorber. Many studies have been done to improve the heat extraction rate of the direct-flow absorber. Heat transfer enhancement has been done by introducing inserts inside the absorber to induce turbulence and increase convective heat transfer. The creation of a turbulent flow using artificial roughness has been proven to enhance the heat transfer process [7]. Ferroni et al. [8] used short twisted-tap inserts, Seemawute & Eiamsa-Ard [9] used alternative axis twisted tape inserts, Thianpong et al. [10] used twisted tape with perforation and Ghadirijafarbeigloo [11] used a perforated louvered twisted tape. Joo et al. [12] concluded that the inserts had an effect of increasing the overall performance, however, twisted tapes increase flow resistance and pressure drop. In a review by Kumar et al. [13] they concluded that increasing the heat transfer coefficient increases the thermal efficiency between the working fluid and absorber tube. Other research works have been done focusing on the enhancement of heat transfer in the absorber by using nano-materials. However, using nano-materials increases the cost of the heating system, and research on the effects of nano-materials on human health is still required [14]. Furthermore, the narrow cross-section and the bent portion of the direct-flow absorbers have been attributed to causing a challenge of the accumulation of nanoparticles on the inner surface of tubes which can cause clogging [15]. The results from all these studies show that increasing the convective heat transfer coefficient has an effect of increasing the heat gained by the ETC. Heat transfer in fluid flow is difficult and complicated to analyze but can be solved by using the combination of the Prandtl number, Nusselt number, and Reynolds number [16]. In a study by Eleiwi et al. [17], they used 5 Reynolds numbers and 3 heat fluxes with varied diameters. A 50 to 250 change in the Reynolds number increased the heat transfer from 6 to 13%.

These studies are based on enhancing heat transfer by optimizing the flow characteristics inside the absorber tube. Another approach is to increase the heat transfer from the borosilicate glass cover to the absorber. This is impacted by the air gap that exists between the absorber tube and the glass cover, which resists heat transfer. Numerous studies have been conducted which seek on increasing the heat transfer surface area, the studies have focused on using fins and solid or liquid filling material between the absorber and the glass cover. Supankanok et al. [18] inserted stainless-steel scrubbers to increase the conduction area through the aluminum fin to the heat pipe. Their results showed an increase in efficiency by 34.96%. Liang et al. [19] used a filled layer and their results showed that the energy gained by ETC is 22% more compared to the copper fin ETC. To improve heat transfer efficiency, the absorber tube's surface area is quite important. Increasing the surface area increases heat transfer. However, this cannot be done by increasing the absorber diameter because the convective heat transfer by the working fluid will reduce thus studies have used filling materials.

The findings from all the different researchers point to 2 general methods of achieving higher performance. That is by increasing the heat transfer surface area of the absorber and improving the convective heat transfer inside the absorber. A limitation is that increasing the convective heat transfer is affected by the pipe diameter, a smaller diameter has better convective heat transfer but reduces the heat transfer surface area. A smaller diameter also may cause clogging when considering nano-materials. A method used in ETC absorbers that can address both 2 methods is the counter-flow mechanism. The counter-flow absorber already exhibits a significant level of fluid mixture and induces turbulence due to the double pipes used which improves convective heat transfer. According to Singh et al. [14], double-pipe heat exchangers are the most advanced type of heat exchanger, they pose a maximum number of quantities and have reduced certain problems up to an extent. The counter-flow absorber also has the advantage of minimizing thermal stresses and maintaining a uniform heat transfer rate. Kim et al. [20] compared the heat pipe, U-tube, and counter-flow ETC with concentrators and

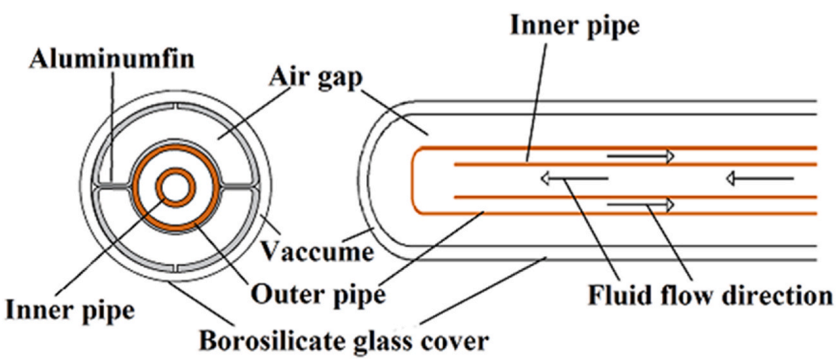

Fig. 1. Schematic of the counter-flow absorber.

found that the counter-flow had better performance above 100 °*C*. This work thus proposes a counter-flow copper absorber for increasing the heat extraction rate and compares its performance to the direct-flow absorber under varied flow rates and heat fluxes. The main objective is to optimize the inner and outer diameter of the counter-flow absorber to increase the convective heat transfer coefficient and to increase the absorber heat transfer surface area for high flow rate systems. Reynolds, Nusselt, and Prandtl numbers are used in the design optimization. The study further compares the proposed counter-flow absorber with the direct-flow absorber performance at varied heat flux. This is necessary because solar concentrators are often used to increase the operating temperature of solar collectors and analysis is required to assess which absorber technology has improved efficiency at higher heat fluxes.

2. Materials and methods

The counter-flow absorber was designed using water as the heat transfer fluid. A schematic showing the counter-flow copper absorber is presented in Fig. 1.

2.1. Fluid flow and convective heat transfer analysis

The heat gained is determined by the convective heat transfer given by Newton's law of cooling, Equation (1).

$$Q_c = h_c A_s \left(T_\infty - T_f\right) \tag{1}$$

The rate of heat transfer is affected by the convective heat transfer coefficient and the collector surface area. Increasing the surface area for heat transfer can be done by increasing the pipe diameter, however, increasing the pipe diameter affects the flow regime. The flow regime can be determined by the Reynolds, Nusselt, and Prandtl numbers. The Reynolds number, Equation (2), is used to determine whether the flow is turbulent or laminar.

$$Re = \frac{4\dot{m}}{\pi D_h \mu} \tag{2}$$

Where the hydraulic diameter of the counter-flow is given by Equation (3).

$$D_h = \frac{\frac{4\pi\left(D_{out}^2 - D_{in}^2\right)}{4}}{\pi(D_{out} + D_{in})} = D_{out} - D_{in} \tag{3}$$

A turbulent flow has better convective heat transfer than a laminar flow due to the existence of a larger boundary layer in laminar flow. The boundary layer acts as insulation and the heat transfer in the fluid is more conduction than convection. The Nusselt number, Equation (4), is used to determine whether heat transfer is conduction or convection.

$$Nu = \frac{h_c D_h}{k} \tag{4}$$

The larger the Nusselt number the more effective the convection. The Nusselt number can also be calculated from Dittus-Boelter, Equation (5).

$$Nu = 0.023 Re^{0.8}\, Pr^{0.4} \tag{5}$$

The Prandtl number gives the ratio of momentum transport to heat transport which is an intrinsic property of the fluid. The convective heat transfer coefficient can be calculated using the Nusselt number from Equations (4) and (5). Equations (1) and (4) can also be combined to give the relationship between the hydraulic diameter, outer diameter, and convective heat transfer, Equation (6). It can be seen that increasing the hydraulic diameter decreases the convection heat transfer while increasing the outer diameter has the opposite effect.

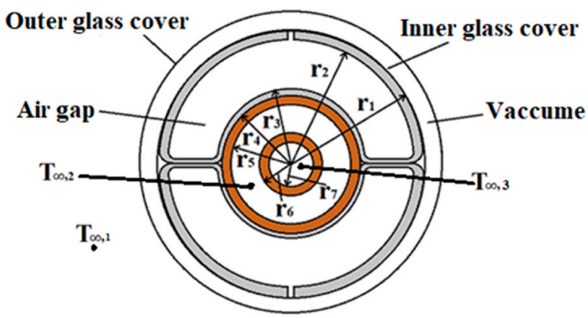

Fig. 2. Cross-section of the counter-flow ETC.

$$Q_c = \frac{D_{out}\pi L N u k_f \left(T_\infty - T_f\right)}{D_h} \tag{6}$$

2.1.1. Heat transfer area analysis

In all the investigations the heat transfer from the surroundings through the vacuum to the outer glass cover will not be considered. Fig. 2 shows a schematic cross-section of the counter-flow ETC. In the schematic r_1; r_2 are the radii of the aluminum fin in contact with the glass cover, r_3; r_4 are the radii of the aluminum fin in contact with the outer copper pipe, r_4; r_5 are the radii of the outer copper pipe and r_6; r_7 are the radii of the inner copper pipe. The heat transfer from the fin to the working fluid can be expressed using the thermal network given in Fig. 3 and Equation (7). In the thermal network, convection and radiation from the fin to the pipe have been combined. Conduction occurs from the aluminum fin to the absorber (copper pipe) then convection occurs between the absorber (copper pipe) and the working fluid.

$$Q = \frac{T_{\infty,1} - T_{\infty,2}}{R_{conv,fin} + R_{cond,fin} + R_{cond,fin} + R_{cond,pipe} + R_{conv,water}} \tag{7}$$

To simplify the analysis the convection and radiation from the fin to the pipe have not been considered. Convection heat transfer to the fluid from the absorber can be removed from the equation for separate analysis. Equation (7) can therefore be reduced to Equation (8) to represent the conductive heat transfer from the fin to the outer copper pipe.

$$Q_{cond} = \frac{T_{\infty,1} - T_{\infty,2}}{\frac{l_{fin}}{A_{fin}k_{fin}} + \frac{\ln\frac{r_3}{r_4}}{2\pi L k_{fin}} + \frac{\ln\frac{r_4}{r_5}}{2\pi L k_{pipe}}} \tag{8}$$

The heat transfer inside the counter-flow absorber can be represented as shown in Fig. 4. The heat gained by water inside the outer pipe is lost to the incoming fluid, pre-heating the incoming fluid. This has the effect of reducing the outlet temperature and reduces the temperature gradient between the outer pipe wall and outflowing fluid. Thus, the heat transfer within the counter-flow should be kept low. The heat transfer within the counter-flow (Q_{count}) can be represented by Equation (9). To reduce the heat loss to the incoming fluid Q_{count} can be decreased by reducing the inner pipe area (A_i). Reducing A_i has an effect of reducing convective heat loss from the outer pipe to the incoming fluid, however the Nusselt number of the inner fluid increases. Furthermore, a material with a lower thermal conductivity and larger pipe thickness can reduce the heat transfer between the 2 flow streams.

$$Q_{count} \frac{T_{\infty,2} - T_{\infty,3}}{\frac{1}{h_{c,o}A_i} + \frac{\ln\frac{r_6}{r_7}}{2\pi L k_{pipe}} + \frac{1}{h_{c,i}A_i}} \tag{9}$$

2.2. Model setup

After the analytical analysis, a model was built-in COMSOL Multiphysics version 5.3a. A 2D-axisymmetrical geometry was built, the material properties were selected from the built-in library, a conjugate heat transfer module was selected in the physics and a stationary study was used. The analysis was done for a single pipe, this was done to assess the absorber performance without the interactions of the header, as the heat transfer in the header may cause stagnation regions [21]. The analysis, therefore, did not produce a complete schematic diagram and complete flow diagram of the counter-flow absorber connected to the header.

The energy extraction rate of the direct-flow and counter-flow absorber is analyzed with an absorber length of 1.5 m for all simulations. The ETC is required to attain medium temperature (140–200 °C), therefore analysis is done for an operating temperature range of up to 200 °C. An analysis is made of temperature gain against flow rate at a varied uniform theoretical heat flux of 1000 W/m^2, 2000 W/$m^{2,}$ and 3000 W/m^2.

The following assumptions were made:

- Steady-state conditions.
- There are no convective heat losses between the absorber and surroundings.
- The length of the pipe is long enough to assume a fully developed flow.
- Heat transfer and flow are both stable.
- No header interactions were considered.

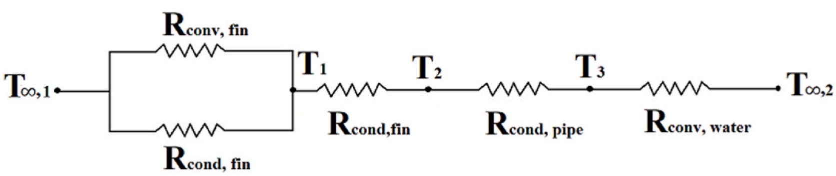

Fig. 3. Thermal network of heat transfer from the outer glass cover to the counter-flow pipe.

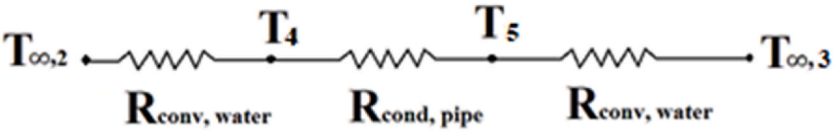

Fig. 4. Thermal network of heat transfer inside the counter-flow pipe.

2.2.1. *Governing equations*

Modeling of the fluid behavior was done using the continuity equation, general heat transfer equations, and an energy equation embedded in COMSOL Multiphysics. A detailed description of the governing equations is found in the COMSOL Heat Transfer Module User's Guide [22]. The equations and boundary conditions are given in Table 1.

2.2.2. *Finite element mesh model*

A physics-controlled mesh was selected for the model shown in Fig. 5. The element size has predefined sizes which start from extremely coarse mesh to extremely fine mesh. The accuracy of the numerical results depends on the mesh size, a mesh analysis was done for flowrate ranges from 0.02 to 0.2 kg/s at a heat flux of 1000 W/m^2. The different mesh sizes selected were coarse mesh, normal mesh, and fine mesh, a grid-dependent test was done and the results are presented in Fig. 6. The difference in the obtained results is very low, to save on computation time all the simulations were meshed with a normal-size mesh. The energy gain by the absorber tube was calculated from Equation (10).

$$Q = \dot{m} C_p (T_2 - T_1) \tag{10}$$

The energy gain per unit area was also analyzed. The energy gain density (S_d) is used to assess the energy gain per absorber area, shown in Equation (11). This however does not represent the instantaneous efficiency because it only takes into account the absorber area and not the aperture area.

$$S_d = \text{Energy gain (MJ / hr)} \,/\, \text{Aperture area } (m^2) \tag{11}$$

2.3. *Model validation*

The model was validated by comparing the simulated results with 2 experimental results by Gao et al. [2] and liang et al. [19]. The results are presented in Tables 2 and 3, there is a little percentage error between the current model and the experimental data. The highest error is 6% and the smallest error is 1.8%. The model is therefore suitable for analysis.

3. Results and discussion

The main objective of the study is to optimize the inner and outer diameter of the counter-flow absorber to increase the convective heat transfer as well as to increase the absorber heat transfer surface area. The results are therefore presented in 3 parts i.e., flow characteristics, absorber surface area, and outlet fluid temperature.

3.1. *Flow characteristics and heat transfer*

The convective heat transfer is assessed using the Nusselt number at both constant flow rate-changing diameter and varied flow rates-varied diameter. The outer diameter for both the counter-flow and direct-flow is varied from 0.02 to 0.07 m. The results are presented in Fig. 7a., the Nusselt number decreases with increased diameter for the direct-flow absorber and remains constant for the counter-flow absorber. The difference in the Nusselt number is from 80 at 0.02 m diameter to 150 at 0.07 m diameter. The constant Nusselt number of the counter-flow absorber is due to the flow characteristics for heat transfer being determined by a hydraulic diameter which is given by $D_{out} - D_{in}$. The hydraulic diameter remains constant while both D_{out} and D_{in} increase. The effect increases

Table 1
Equations and Boundary conditions.

Boundary	Boundary condition	Equations
Pipe inlet	Temperature	$T = T_o \; u = -U_o \; n$
	Mass flow rate	$-\int_{\partial\Omega} \rho(u.n) d_{bc} ds = m$
Wall	Heat flux	$-n.q = q_o \; u = 0$
	Diffuse surface	$-n.q = \varepsilon\delta \, (T_{amb}^4 - T^4)$
	No slip condition	$\varepsilon = 0.05$
Pipe outlet	Outflow	$-n.q = q_o \; n^T \left[-pi + \mu\left(\nabla u + (\nabla u)^T - -\frac{2}{3}\mu(\nabla.u)I\right)\right] n = -\widehat{p}_o$
	Pressure	
	Velocity	$\widehat{p}_o \leq p_o, u.t = 0$

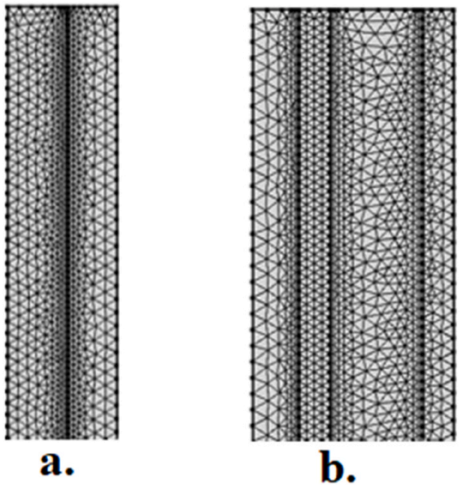

Fig. 5. Different mesh elements for a. direct-flow absorber and b. counter-flow absorber.

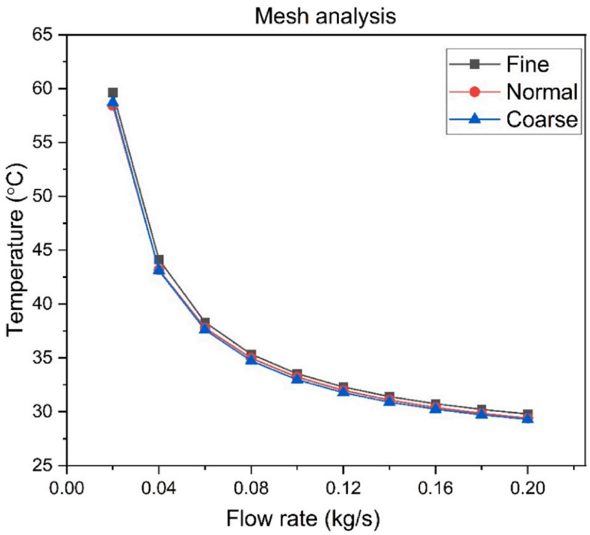

Fig. 6. Grid-dependent test.

Table 2
Comparison of the model results with experimental results by Gao et al. [2].

Flow rate (kg/s)	Heat flux (W/m^2)	Tin)	Tout) (Gao et al.)	Tout) Current model	Error
0.01	926	22.9	29	30.905	6
0.03	860	56.6	61	63.281	3.6

Table 3
Comparison of the model results with experimental results by Liang et al. [20].

Flow rate (kg/s)	Heat flux (W/m^2)	Tin)	Tout) (Liang et al.)	Tout) Current model	(%) Error
0.03	900	35	43	41	4.6
0.04	900	35	41	40	2.4
0.05	900	35	40	39	2.5
0.06	900	35	39	38	2.5
0.07	900	35	38.5	37.8	1.8
0.08	900	35	38	37.4	1.6

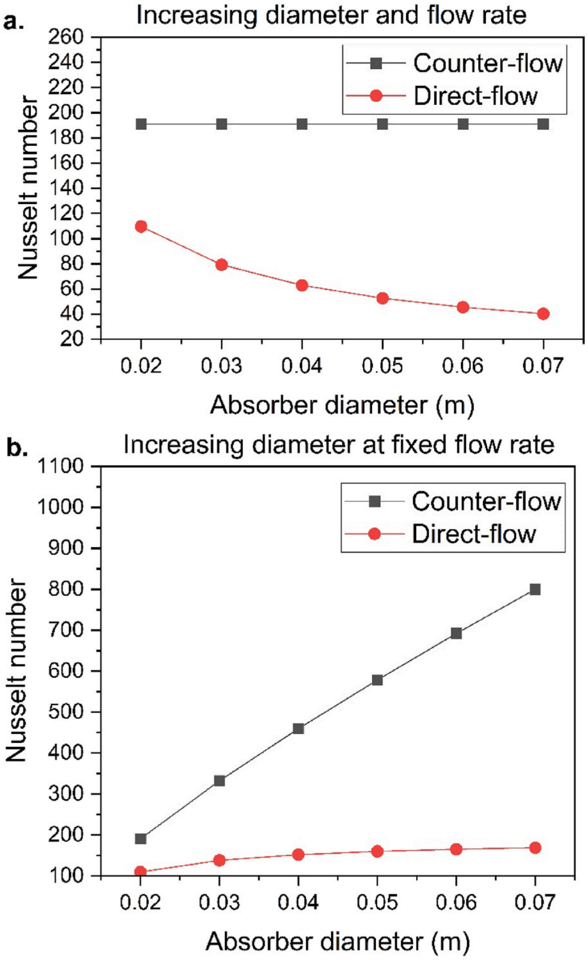

Fig. 7. Changes of Nusselt number with changes in diameter and flow rate.

the heat transfer area while maintaining the Nusselt number constant. The ETC having maximum absorbing surface provides better performance. For the direct-flow absorber, the heat transfer area increases but the Nusselt number also decreases.

The absorber diameter was increased from 0.02 to 0.7 m, and as the diameter was increased the flow rate was also increased from 0.04 to 0.24 kg/s. The results are presented in Fig. 7b. The Nusselt number and heat transfer area increase for both the counter-flow and direct-flow absorbers, however, the counter-flow absorber has a steeper gradient. It can be observed that the magnitude of the difference between the Nusselt number of the counter-flow and direct-flow increases with an increase in flow rate. The difference in the Nusselt number is from 80 at 0.02 m to 650 at 0.07 m. This suggests that at lower flow rates the difference in convective heat transfer will not be too large as compared to higher flow rates.

From the analyzed diameters a smaller diameter has the highest *Nu* number for the direct-flow absorber and the *Nu* number remained constant for any increase in diameter for the counter-flow absorber as long as the hydraulic diameter remained constant. The Nusselt number was assessed at a fluid temperature of 80 and 200 $^{\circ}C$ for varied flow rates. The diameters were fixed at 0.02 m for the counter-flow absorber and 0.01 m for the direct-flow absorber. The results are shown in Fig. 8, the Nusselt number for both the counter-flow and direct-flow increases with increased flow rates. At 80 $^{\circ}C$ the difference in Nusselt number ranges from 40 at 0.04 kg/s to 160 at 0.24 kg/s while that at 200 $^{\circ}C$ ranges from 81 to 341 for the same flow rate ranges. The difference is relatively smaller at a lower temperature compared to a higher temperature for the same flow rate. The convective heat transfer was calculated and the results are shown in Fig. 9. A similar trend is observed where the convective heat transfer increases with an increased flow rate. The magnitude of the difference in convective heat transfer between the counter-flow and direct-flow absorber increases from 93 kW to 391 kW from a flow rate range of 0.04 kg/s to 0.24 kg/s. Although the magnitude of the difference increases a 50% difference is maintained from the flow rate range. In Fig. 8b., when the temperature difference changes from 5 to 165 $^{\circ}C$ the difference in convective heat transfer increases from 70% to 97%.

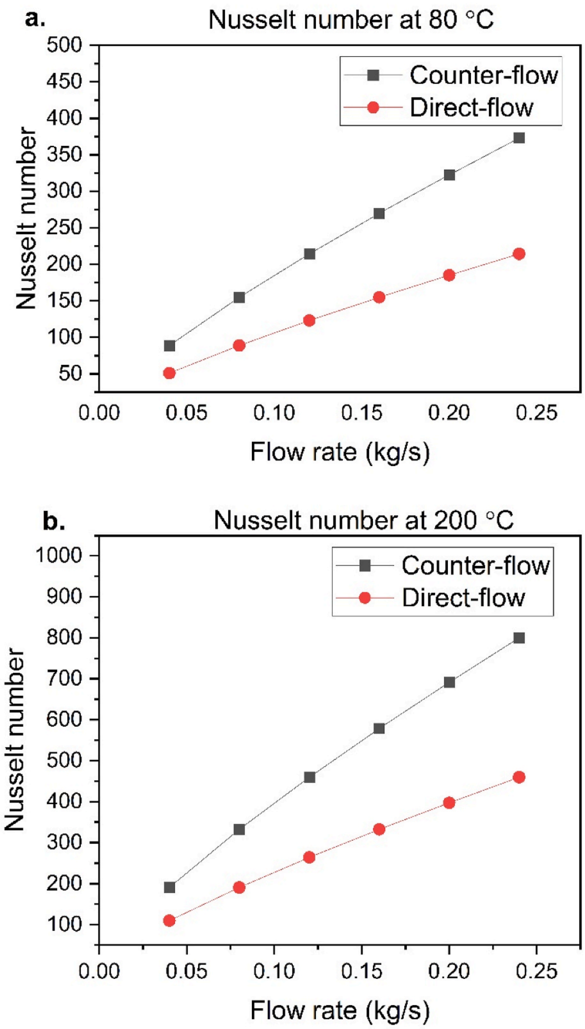

Fig. 8. Changes in *Nu* number at varied flow rates.

3.2. Effect of absorber area on conductions

An analysis of the effect of the pipe diameter on heat transfer is presented in this section. Fig. 10 a and b show the cross-sectional area of the counter-flow and direct-flow absorber with the associated dimensions of the fin and borosilicate glass cover. The properties of the copper pipe and fin are given in Table 4.

The conduction heat rate is calculated for the varied temperature difference between the fin and the copper absorber. The results are presented in Fig. 11. The difference in conductive heat transfer increases from 2.8 to 14.2 W for a change in temperature from 1 to 5 $^{\circ}C$. The difference in the pipe diameter (0.02 m for the counter-flow absorber and 0.01 m for the direct-flow absorber) gives a 36% difference in the conductive heat transfer. A simulation was made to assess the temperature contours, the results are presented in Fig. 12.

The temperature profile in the contour shows that there is a larger temperature difference between the absorber wall and the fluid for the counter-flow absorber compared to the direct-flow. A large temperature difference increases the heat transfer and efficiency of the counter-flow absorber. Mehla & Kumar [24] found that the maximum mean collector efficiency was high for a circular fin with counter-flow at high flow rates compared to parallel flow. They state that the increase in efficiency was due to the high fluid temperature difference.

3.3. Temperature and energy gain analysis

Analysis was done for the outlet temperature and overall heat gain of the absorbers. A conjugate heat transfer model was used in COMSOL Multiphysics 5.3a for all the simulations.

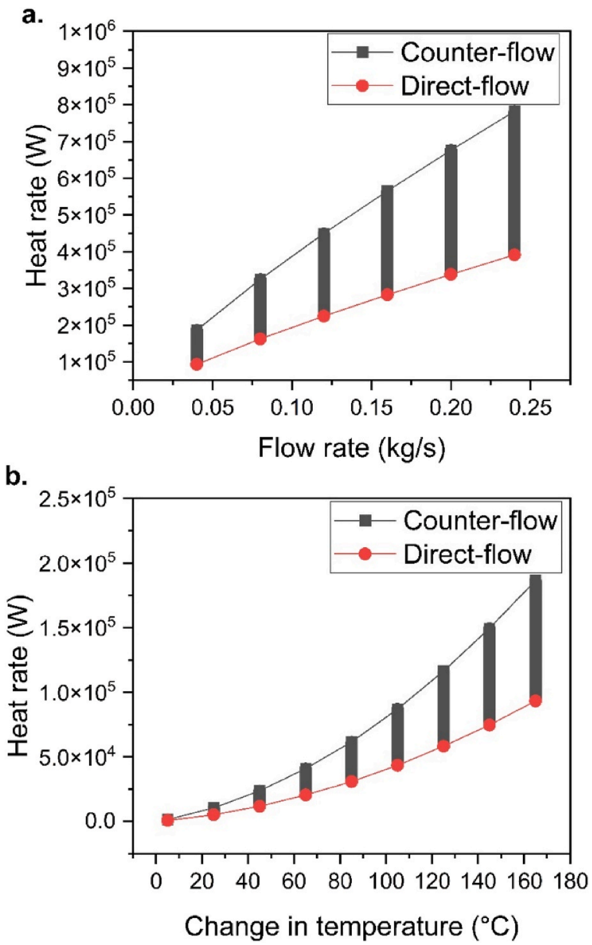

Fig. 9. Difference in convection heat transfer at varied a. flowrate and b. temperature.

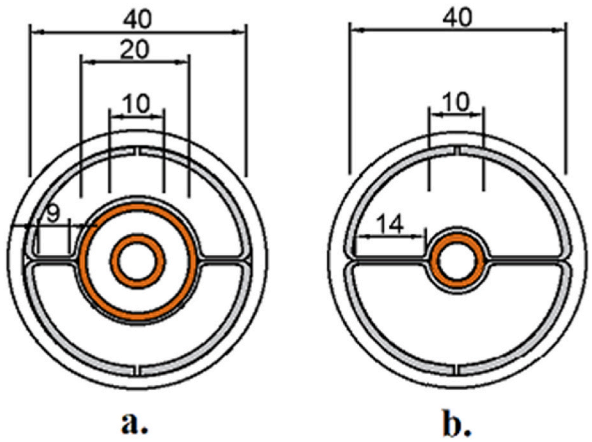

Fig. 10. Cross-section of a. counter-flow absorber and b. direct-flow absorber.

3.3.1. Changes in absorber diameter W/m^2

The effects of the inner and outer diameters were assessed. The different inner diameters of the counter-flow absorber were fixed at 0.01, 0.015, 0.02, and 0.03 m while the outer diameter was varied from 0.04 m to 0.14 m. The diameter of the direct-flow was varied from 0.01 to 0.14 m. The heat flux for both absorbers was set at 1000 W/m^2 and the results are presented in Fig. 13. The energy gain by the direct-flow absorber decreases with an increase in diameter while the energy gain by the counter-flow absorber increases with an

Table 4
Material properties of the absorbers.

Property	Counter-flow	Direct-flow
(Copper)	386 W/m^2	386 W/m^2
(Aluminum)	239 W/m^2	239 W/m^2
	0.009 m	0.014 m
Fin thickness	0.0002 m	0.0002 m
(Length of absorber)	1.5 m	1.5 m
(Outer radius of fin)	0.0212 m	0.0112 m
(Inner radius of fin)	0.021 m	0.011 m
(Inner radius of absorber)	0.02 m	0.01 m

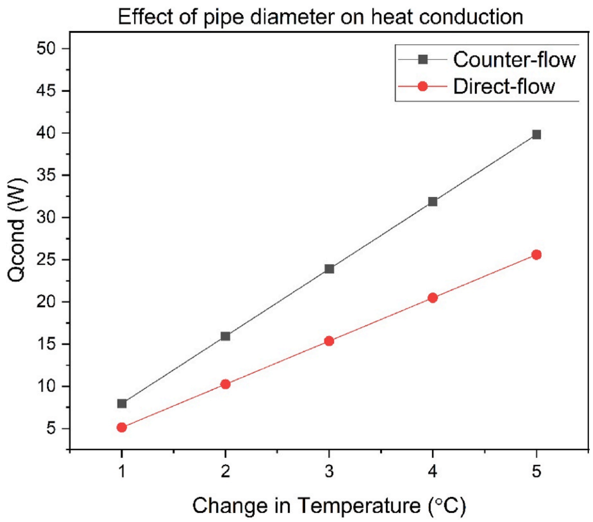

Fig. 11. Conductive heat transfer at varied temperatures.

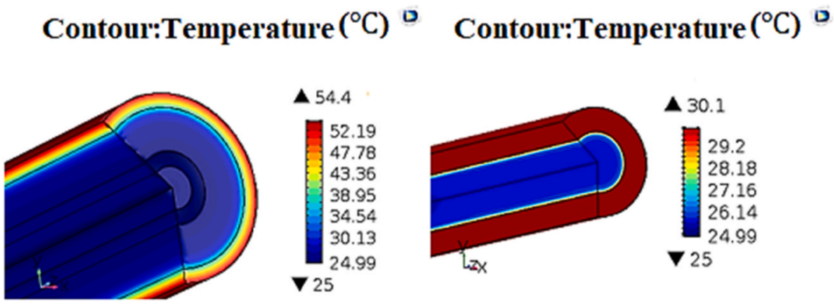

Fig. 12. Temperature contours of a. counter-flow absorber and b. direct-flow absorber.

increase in the outer diameter. However, there is a restriction on the diameter of 0.05 m for practical applicability with a borosilicate evacuated glass cover. The direct-flow absorber, therefore, has better performance than the counter-flow absorbers with an inner diameter of 0.03 and 0.02 m. However, the counter-flow with inner diameters of 0.01 and 0.015 m has better performance than the direct-flow absorber. The most optimum diameter for the counter-flow can be chosen to be 0.01 and 0.04 m inner and outer diameter respectively. However, an outer diameter of 0.02 m may be chosen to reduce the cost of purchasing a higher-diameter copper pipe. The counter-flow with 0.01 and 0.02 m inner and outer diameter respectively has 4 times more energy gain than the direct-flow with 0.01 m diameter. When $D_{in} > D_{out} - D_{in}$ there is more heat loss from the out outgoing fluid to the incoming fluid. When $D_{out} - D_{in} > 4\dot{m}/(\pi 4000\mu)$ the Reynolds number will be lower than 4000 hence low convective heat transfer. It follows that the optimum diameter of the counter-flow can be optimized by the simple expression $D_{in} \leq D_{out} - D_{in} < 4\dot{m}/(\pi 4000\mu)$.

3.3.2. Material properties

The material properties of the inner pipe were assessed. The heat transfer rate from the outside pipe to the working fluid can be

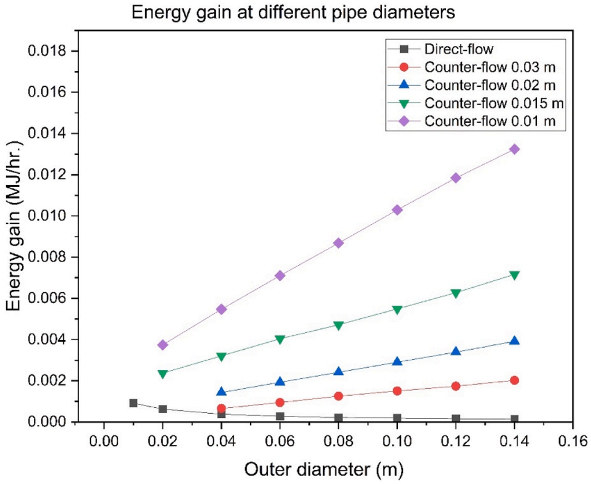

Fig. 13. Energy gain by the direct-flow and counter-flow at different diameters.

increased by using a material with high thermal conductivity. Conversely, a material with low thermal conductivity is required to reduce the heat loss from the outgoing fluid to the incoming fluid. Copper was used for the outer pipe with a thermal conductivity of 386 W/m^{2}K. A comparison was made between copper and steel with a thermal conductivity of 44.5 W/m^{2}K for the inner diameter. An analysis was also made for changes in pipe thickness to increase the thermal conductive resistance. The results show that changing the thickness of copper from 0.00124 m to 0.00241 m (schedule 10 to schedule 80 pipes) at a low flow rate of 0.02 kg/s had a change in outlet temperature of 2.3, 3.1 and 3.4% for heat fluxes of 1000, 2000 and 3000 W/m^2 respectively. A comparison of copper 0.00124 m thick and steel 0.00241 m gave a difference in outlet temperature of 4, 6, and 7% for the same operating conditions. However, at flow rates >0.1 kg/s the difference in the outlet temperature was <1% for all the heat fluxes. Although the % difference was low the results show that the counter-flow can be designed using a cheaper material than copper for the inner pipe.

3.3.3. *Changes in heat flux*

Heat fluxes of 1000, 2000, and 3000 W/m^2 are considered for the direct-flow and counter-flow absorber, the results are given in Fig. 14. There is an increase in temperature for both the counter-flow and direct-flow absorbers at increased heat flux. However, as the flow rate is increased the temperature drops significantly for the direct-flow absorber compared to the counter-flow absorber. The increase in temperature for the direct-flow from 1000 to 2000 W/m^2 is 23% at a flow rate of 0.02 kg/s and reduces to 4% at a flow rate of 0.2 kg/s while that from 1000 to 3000 W/m^2 is 47% and drops to 7%. At the same operating conditions, the counter-flow has an increase of 53% and drops to 13%, 104%, and drops to 26%. The magnitude of the temperature change from 1000 W/m^2 doubling to 2000 W/m^2 and tripling to 3000 W/m^2 can be summarized in Table 5.

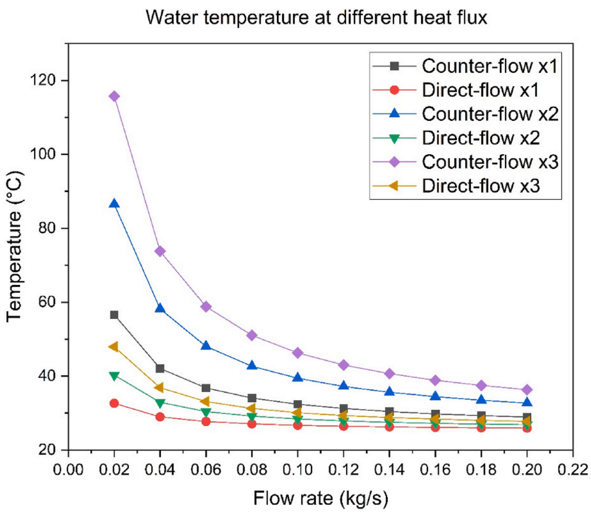

Fig. 14. Temperature profile of the direct-flow absorber and counter-flow absorber at different heat flux and flow rates.

Table 5
Magnitude of temperature changes with change in heat flux.

Flow rate (kg/s)	Magnitude of temperature increment from 1000 W/m^2			
	Direct-flow 2000 W/m^2	Counter-flow 2000 W/m^2	Direct-flow 3000 W/m^2	Counter-flow 3000 W/m^2
0.02	1.2	1.5	1.5	2
0.2	1.04	1.1	1.07	1.4

3.3.4. Area usage analysis

The counter-flow absorber presented has a larger diameter than the direct-flow hence the energy gained per area becomes of importance. This can be assessed using the solar energy gain density (S_d) presented in Table 6. The S_d was calculated at heat fluxes of 1000 and 3000 W/m^2. The energy density for the counter-flow absorber is higher than the direct-flow in all the cases. Furthermore, the counter-flow at 3000 W/m^2 can have an energy gain from 3.6 to 3.8 times higher than the direct-flow ETC at 1000 W/m^2.

4. Conclusion

The proposed counter-flow copper absorber presents a better heat extraction rate than the direct-flow absorber at higher flow rates which are required in industrial heating. The counter-flow absorber allows for an increment in the pipe diameter which cannot be done by the direct-flow absorbers. The results presented show a similar trend to the work of Naik et al. [25] for changes in flow rate with outlet temperature. There is also conformity with the work of Eleiwi et al. [18] for performance improvement from an increased Reynolds number.

The main results of this study are summarized as follows:

1 The counter-flow absorber allows increasing the heat transfer surface area without affecting the flow regime. The flow regime is independently affected by the hydraulic diameter while the surface area is affected by the outer diameter. The outer diameter can be increased to give a desired surface area while the hydraulic diameter is maintained to give the most optimum flow characteristics. The counter-flow with a 0.01 and 0.02 m inner and outer diameter has 4 times more energy gain than the direct-flow with a 0.01 m diameter.
2 When designing the counter-flow absorber the most optimum diameters can be derived by the simple expression $D_{in} \leq D_{out} - D_{in} < 4\dot{m}/(\pi 4000\mu)$ and the inner diameter should have a low thermal conductivity and larger thickness.
3 The counter-flow absorber has higher performance at a high flow rate and higher temperature range. The magnitude of the difference in convective heat transfer between the counter-flow and direct-flow absorber increases from 93 kW to 391 kW from a flow rate range of 0.04 kg/s to 0.24 kg/s. The difference in the Nusselt number between the counter-flow and direct-flow increases with an increase in temperature. When the temperature difference between the surface and the fluid changes A temperature difference of 5 °C–165 °C between the surface and the fluid gives a convective heat transfer rise of 70%–97%. Hence at increased temperatures, the magnitude of the Nusselt number is very high and significantly affects the heat transfer rate. This conforms with the observations by Kim et al. [20].
4 Doubling the heat flux at flow rate ranges of 0.02 kg/s and 0.2 kg/s increases the temperature by 1.5 and 1.1 for the counter-flow absorber and by 1.2 and 1.04 for the direct-flow absorber. Tripling the heat flux at flow rate ranges of 0.02 kg/s and 0.2 kg/s increases the temperature by 2 and 1.4 for the counter-flow absorber and by 1.5 and 1.07 for the direct-flow absorber.

Further studies are proposed as follows:

1. The analysis done was limited to heat transfer in the absorber and did not consider the header. Design of a specialized header for the counter-flow absorber is thus required.
2. To analyze the counter-flow absorber using different heat transfer fluids.

Table 6
S_d of counter-flow absorber and direct-flow absorber at 3000 W/m.^{2}.

Flowrate (kg/s)	Counter-flow at 3000 W/m^2	Direct-flow at 3000 W/m^2	Direct-flow at 1000 W/m^2	Counter-flow at 1000 W/m^2
	S_d (MJ/hr.m^2)	S_d (MJ/hr.m^2)	S_d (MJ/hr.m^2)	S_d (MJ/hr.m^2)
0.02	0.029	0.024	0.008	0.010
0.04	0.032	0.025	0.008	0.011
0.06	0.033	0.026	0.009	0.011
0.08	0.034	0.026	0.009	0.012
0.10	0.034	0.027	0.009	0.012
0.12	0.035	0.027	0.009	0.012
0.14	0.035	0.028	0.009	0.012
0.16	0.036	0.028	0.009	0.012
0.18	0.036	0.029	0.010	0.013
0.20	0.037	0.029	0.010	0.013

3. To analyze the counter-flow absorber with a solid or fluid filling between the air gap and absorber tube.

Author contribution statement

Downmore Musademba: conceived and designed the experiments; analyzed and interpreted the data; Contributed reagents, materials, analysis tools or data.
Shaibu Tambula: conceived and designed the experiments; performed the experiments; analyzed and interpreted the data; wrote the paper.
Chido H. Chihobo: conceived and designed the experiments; performed the experiments; wrote the paper.

Funding statement

Downmore Musademba was supported by the Research Council of Zimbabwe and Zimbabwe Energy Regulatory Authority Grant ID: ref sc-18-24.

Data availability statement

Data will be made available on request.

Declaration of interest's statement

The authors declare no competing interests.

Acknowledgments

We would like to acknowledge the Research Council of Zimbabwe and the Zimbabwe Energy Regulatory Authority for their financial support, grant ID: ref sc-18-24.

Nomenclature

A_s	Surface area (m^2)
r_{1-7}	Radius at a specified point (m)
A_i	Inner pipe area (m^2)
Q	Useful Energy gain by the water (W)
A_o	Outer pipe area (m^2)
Q_c	Rate of heat transfer (W)
C_p	Specific heat capacity of water (kJ/kg.K)
Q_{cond}	Rate of conductive heat transfer (W)
D_h	Hydraulic diameter (m)
q_o	Inward heat flux (W/m^2)
D_{out}	Outer diameter (m)
q	Conductive heat flux (W/m^2)
D_{in}	Inner diameter (m)
Re	Reynolds number
h_c	Convective heat transfer coefficient (W/m^2K)
S_d	Energy gain density ($MJ/hr.m^2$)
k	Thermal conductivity (W/m.K)
T	Temperature ($^\circ C$)
L	Length of absorber (m)
T_o	Equilibrium temperature ($^\circ C$)
l_{fin}	Length of fin (m)
T_∞	Temperature of the surroundings ($^\circ C$)
$\dot{m}$	Mass flowrate (kg/s)
$T_{\infty,1}$	Temperature of the fluid at specified point ($^\circ C$)
u	Fluid velocity vector (m/s)
$T_{\infty,2}$	Temperature of the fluid in the outer pipe ($^\circ C$)
n	Normal vector toward exterior
$T_{\infty,3}$	Temperature of the fluid in the inner pipe ($^\circ C$)
Nu	Nusselt number
μ	Dynamic viscosity (Pa.s)

Pr	Prandtl number
ε	Surface emissivity
pi	Density of thin rod (kg/m^3)
δ	Vapor permeability of still air (s)
p_o	Heat rate (W)
ds	Thickness of shell or thin layer (m)
ρ	Density (kg/m^3)
∂Ω	Geometry domain's boundaries
R	Thermal resistance (K/W)

References

[1] M.A. Sabiha, R. Saidur, S. Mekhilef, O. Mahian, Progress and latest developments of evacuated tube solar collectors, Renew. Sustain. Energy Rev. 51 (2015) 1038–1054, https://doi.org/10.1016/j.rser.2015.07.016.

[2] Y. Gao, et al., Thermal performance and parameter analysis of a U-pipe evacuated solar tube collector, Sol. Energy 107 (2014) 714–727, https://doi.org/10.1016/j.solener.2014.05.023.

[3] A. Yadav, V.K. Bajpai, Thermal performance of one-ended evacuated tube solar air collector at different flow rates: experimental investigation, Int. J. Ambient Energy 33 (1) (2012) 35–50, https://doi.org/10.1080/01430750.2011.636207.

[4] X. Zhang, et al., Thermal performance of direct-flow coaxial evacuated-tube solar collectors with and without a heat shield, Energy Convers. Manag. 84 (2014) 80–87, https://doi.org/10.1016/j.enconman.2014.04.014.

[5] S. Praful, V.P. Rao, V. Vijeth, S.V. Bhagavath, K.N. Seetharamu, R.N. Rao, On the operating temperature of heat pipes, J. Phys. Conf. Ser. 1473 (1) (2020), https://doi.org/10.1088/1742-6596/1473/1/012025.

[6] C. Jiang, et al., A review of the compound parabolic concentrator (CPC) with a tubular absorber, Energies 13 (3) (2020), https://doi.org/10.3390/en13030695.

[7] A.S. Abdullah, M.M.A. Al-sood, Z.M. Omara, M.A. Bek, A.E. Kabeel, Performance evaluation of a new counter fl ow double pass solar air heater with turbulators, Sol. Energy 173 (2018) 398–406, https://doi.org/10.1016/j.solener.2018.07.073.

[8] P. Ferroni, R.E. Block, N.E. Todreas, A.E. Bergles, Experimental evaluation of pressure drop in round tubes provided with physically separated, multiple, short-length twisted tapes, Exp. Therm. Fluid Sci. 35 (7) (2011) 1357–1369, Oct, https://doi.org/10.1016/j.expthermflusci.2011.05.004.

[9] P. Seemawute, S. Eiamsa-Ard, Visualization of flow and heat transfer in tube with twisted tape consisting of alternate axis, 4th Int. Conf. Comp. Model. Simulat. 22 (2012) 36–40.

[10] C. Thianpong, P. Eiamsa-Ard, S. Eiamsa-Ard, Heat transfer and thermal performance characteristics of heat exchanger tube fitted with perforated twisted-tapes, Heat Mass Transfer/Waerme- und Stoffuebertragung 48 (6) (2012) 881–892, https://doi.org/10.1007/s00231-011-0943-0.

[11] S. Ghadirijafarbeigloo, A.H. Zamzamian, M. Yaghoubi, 3-D numerical simulation of heat transfer and turbulent flow in a receiver tube of solar parabolic trough concentrator with louvered twisted-tape inserts, Energy Proc. 49 (2014) 373–380, https://doi.org/10.1016/j.egypro.2014.03.040.

[12] H.-J. Joo, H.-Y. Kwak, M. Kong, Effect of twisted tape inserts on thermal performance of heat pipe evacuated-tube solar thermal collector, Energy (2022), 124307.

[13] A. Kumar, Z. Said, E. Bellos, An up-to-date review on evacuated tube solar collectors, J. Therm. Anal. Calorim. 145 (6) (2021) 2873–2889, https://doi.org/10.1007/s10973-020-09953-9.

[14] S.K. Singh, M.K. Chauhan, A.K. Shukla, Heat transfer enhancement in double-pipe heat exchanger: a review, J. Phys. Conf. Ser. 2178 (1) (2022), https://doi.org/10.1088/1742-6596/2178/1/012007.

[15] N. Choudhary, D.K. Sharma, A. Nayyar, A mini review on the design modifications in evacuated tube solar collectors to improve the performance and productivity, SKIT Res. J. 11 (2) (2021) 66, https://doi.org/10.47904/ijskit.11.2.2021.66-70.

[16] M.R. Noor, N. Syafiqah, H. Mohd, S. Nur, F. Masrom, Graphing behaviour of heat transfer in terms of Nusselt and Reynolds, J. Comput. Res. Innovat. (JCRINN) 6 (2) (2021) 41–52.

[17] M.A. Eleiwi, T.A. Tahseen, A.F. Hameed, Numerical study of fluid flow and heat transfer in a backward facing step with three adiabatic circular cylinder, J. Advan. Res. Fluid Mech. Thermal Sci. 72 (1) (2020) 80–93, https://doi.org/10.37934/arfmts.72.1.8093.

[18] R. Supankanok, S. Sriwong, P. Ponpo, W. Wu, W. Chandra-Ambhorn, A. Anantpinijwatna, Modification of a solar thermal collector to promote heat transfer inside an evacuated tube solar thermal absorbe, Appl. Sci. 11 (9) (2021), https://doi.org/10.3390/app11094100.

[19] R. Liang, L. Ma, J. Zhang, D. Zhao, Experimental study on thermal performance of filled-type evacuated tube with U-tube, Heat and Mass Transfer/Waerme- und Stoffuebertragung 48 (6) (2012) 989–997, https://doi.org/10.1007/s00231-011-0912-7.

[20] Y.S. Kim, K. Balkoski, L. Jiang, R. Winston, Efficient stationary solar thermal collector systems operating at a medium-temperature range, Appl. Energy 111 (2013) 1071–1079, https://doi.org/10.1016/j.apenergy.2013.06.051.

[21] G.L. Morrison, I. Budihardjo, M. Behnia, Measurement and simulation of flow rate in a water-in-glass evacuated tube solar water heater, Sol. Energy 78 (2) (2005) 257–267, https://doi.org/10.1016/j.solener.2004.09.005.

[22] C. Multiphysics, Heat Transfer Module," © 1998–2018 Comsol, 2015, pp. 1–222 [Online]. Available: https://doc.comsol.com/5.4/doc/com.comsol.help.heat/HeatTransferModuleUsersGuide.pdf.